ACS APPLIED MATERIALS & INTERFACES

Research Article

Cite This: ACS Appl. Mater. Interfaces 2019, 11, 18960−18967

www.acsami.org

Atomically Flat Au Nanoplate Platforms Enable Ultraspecific Attomolar Detection of Protein Biomarkers

Ahreum Hwang,[†,‡,¶] Eungwang Kim,[†,‡,¶] Jeong Moon,[‡,§] Hyoban Lee,[†] Miyeon Lee,[†] Jinyoung Jeong,[∥,⊥] Eun-Kyung Lim,[‡,∥] Juyeon Jung,[‡,∥] Taejoon Kang,*[,‡,∥] and Bongsoo Kim*[,†]

[†]Department of Chemistry and [§]Department of Chemical and Biomolecular Engineering, KAIST, Daejeon 34141, Korea

[‡]Bionanotechnology Research Center and [⊥]Environmental Disease Research Center, KRIBB, Daejeon 34141, Korea

[∥]Department of Nanobiotechnology, KRIBB School of Biotechnology, UST, Daejeon 34113, Korea

Supporting Information

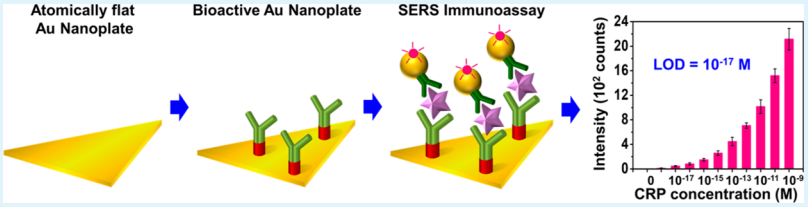

ABSTRACT: Atomically flat surfaces of single-crystalline Au nanoplates can maximize the functionality of biomolecules, thus realizing extremely high-performance biosensors. Here, we report both highly specific and supersensitive detection of C-reactive protein (CRP) by employing atomically flat Au nanoplates. CRP is a protein biomarker for inflammation and infection and can be used as a predictive or prognostic marker for various cardiovascular diseases. To maximize the binding capacity for CRP, we carefully optimized the Au nanoplate-Cys3-protein G-anti-CRP structure by observing atomic force microscopy (AFM) images. The optimally anti-CRP-immobilized Au nanoplates allowed extremely specific detection of CRP at the attomolar level. To confirm the binding of CRP onto the Au nanoplate, we assembled Au nanoparticles (NPs) onto the CRP-captured Au nanoplate by sandwich immunoreaction and obtained surface-enhanced Raman scattering (SERS) spectra and scanning electron microscopy (SEM) images. Both the SERS and SEM results showed that we completely eliminated the nonspecific binding of Au NPs onto the optimally anti-CRP-immobilized Au nanoplate. Compared with the anti-CRP-immobilized rough Au film and the randomly anti-CRP-attached Au nanoplate, the optimally anti-CRP-immobilized Au nanoplate provided a highly improved detection limit of 10^{-17} M. In this study, it was validated that ultraclean and ultraflat Au nanoplates can maximize the sensing capability of CRP. We expect that these Au nanoplates will enable the feasible detection of many important biomarkers with high specificity and high sensitivity.

KEYWORDS: *atomically flat, gold, nanoplate, antibody immobilization, C-reactive protein, surface-enhanced Raman scattering*

1. INTRODUCTION

Atomically flat surfaces of nanomaterials have been employed to establish effective interfaces with various systems, thus innovatively improving nanomaterial-based devices.[1,2] For example, atomically flat surfaces can exhibit advanced performances for optical and electronic devices because the surfaces can significantly reduce the scattering loss of photons and electrons.[3−5] In the development of high-performance biological sensors, it is critical to construct optimally bioactive surfaces that can maximize the functionality of immobilized molecules onto the surfaces.[6] Atomically flat and ultraclean Au nanoplates are promising materials for these bioactive surfaces because biological molecules can be uniformly and optimally immobilized on Au surfaces.[7] As a first step toward the construction of optimally bioactive Au surfaces, we previously reported the synthesis of single-crystalline Au nanoplates in the vapor phase.[7] The synthesized Au nanoplates are ultraflat and ultraclean and have no grain boundaries.[7] Because these superior properties of single-crystalline Au nanoplates have improved the biological sensing performance, Au nanoplates have emerged as novel building blocks for high-performance biological sensors.[8]

For the realization of high-performance biosensors employing Au nanoplates, an important task to complete is the dense, homogeneous, and stable immobilization of bioreceptors onto Au surfaces.[9] Among many kinds of bioreceptors, antibodies have been the most widely used for the detection of biomolecules.[10,11] To maximize the binding capacity of an antibody against an antigen, it should be immobilized on the Au surface uniformly with an optimal orientation.[12] In particular, the oriented immobilization of the antibody is highly important so that the antibody has the optimal conformation for its interaction with the antigen.[13] Previous studies suggested that a well-ordered antibody could improve

Received: March 11, 2019
Accepted: May 7, 2019
Published: May 7, 2019

DOI: 10.1021/acsami.9b04363
ACS Appl. Mater. Interfaces 2019, 11, 18960−18967

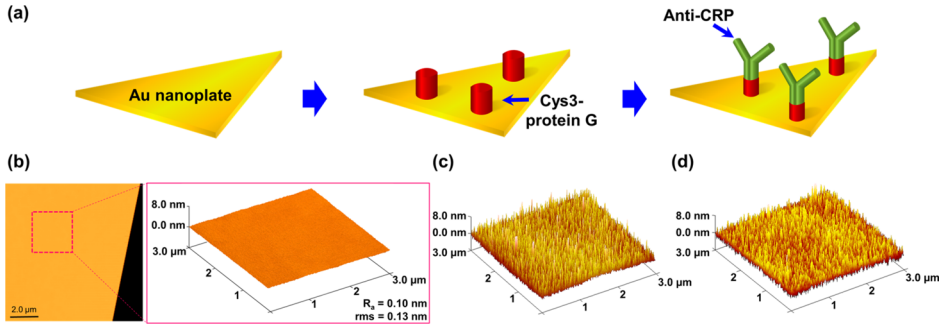

Figure 1. (a) Schematic illustration of anti-CRP immobilization onto an Au nanoplate. (b) AFM image of an atomically flat Au nanoplate. (c) AFM image of a Cys3-protein G-immobilized Au nanoplate. (d) AFM image of an anti-CRP-immobilized Au nanoplate.

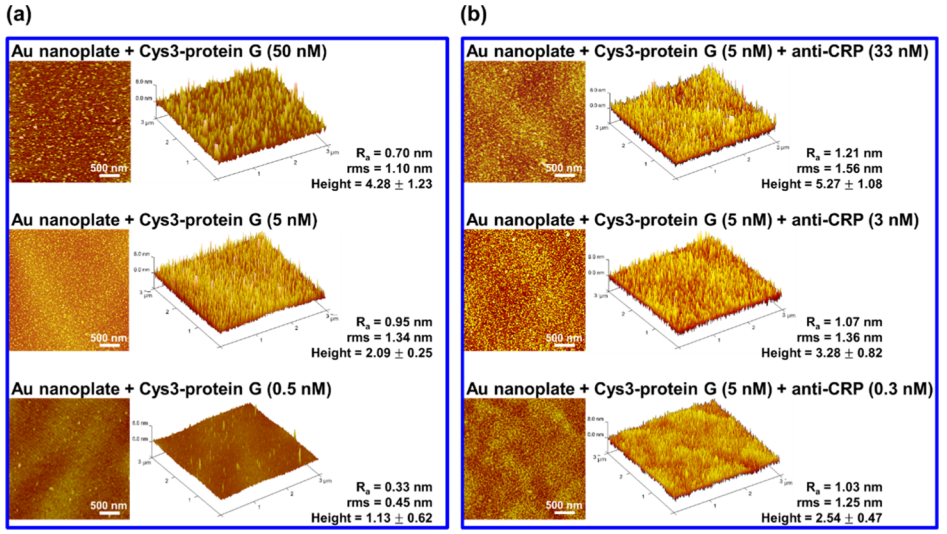

Figure 2. (a) AFM images of Cys3-protein G-immobilized Au nanoplates by varying the concentration of Cys3-protein G from 0.5 to 50 nM. (b) AFM images of anti-CRP-immobilized Au nanoplates by varying the concentration of anti-CRP from 0.3 to 33 nM.

the antigen binding capacity by up to 8-fold over that of the random-ordered antibody.[14] Various antibody immobilization techniques have been developed by employing adsorption, covalent bonding, antibody tagging, antibody binding proteins, recombinant antibodies, and so forth.[15] Among these techniques, antibody binding proteins such as proteins G,[12−14] A,[16] and L[17] have been frequently used because they can effectively expose the binding site of the antibody to the antigen. Therefore, we tried to uniformly modify protein G onto the Au nanoplate and then immobilize the antibody onto the Au nanoplate sequentially for the construction of the optimal antibody-immobilized Au surface. The optimally immobilized antibody on the ultraflat and ultraclean Au nanoplate may enable the realization of a high-performance biosensor.

As a proof-of-concept, we immobilized the antibody against C-reactive protein (CRP) onto the Au nanoplates in an optimal orientation and applied them to CRP detection. CRP is a well-characterized biomarker for inflammation and is an independent predictor of future cardiovascular events.[18,19] Moreover, accumulating evidence suggests that the CRP level is implicated in the development of type 2 diabetes mellitus and the pathogenesis of metabolic syndrome.[20,21] Therefore, it is important to detect CRP in a highly sensitive and specific manner.[22,23] To fabricate a Au surface with maximum binding capacity for CRP, we carefully optimized the Au nanoplate-Cys3-protein G-anti-CRP structure under atomic force microscopy (AFM) observation. After the optimal immobilization of protein G and anti-CRP onto the Au nanoplates, CRP detection was accomplished. In particular, we employed the anti-CRP-attached Au nanoparticle (NP) as a probe for the confirmation of CRP binding onto the optimally anti-CRP-immobilized Au nanoplate. The Au NPs were assembled onto the Au nanoplate in the presence of only CRP, leading to the formation of the NPs-on-nanoplate architecture. The CRP-detected NPs-on-nanoplate structure was clearly observed by scanning electron microscopy (SEM) measurements. Moreover, we quantitatively analyzed CRP by measuring the surface-enhanced Raman scattering (SERS) signals, which are strongly enhanced in the nanogap of the NPs-on-nanoplate structure.[1,7,8,24] As a result, 10^{-17} M of CRP was detectable using the optimally anti-CRP-immobilized Au nanoplate. Furthermore, the optimally anti-CRP-immobilized Au nanoplate did not interact with proteins other than CRP, and it completely suppressed the nonspecific binding of Au NPs. Through comparative experiments with an anti-CRP-immobilized rough Au film and a randomly anti-CRP-attached Au nanoplate, it was determined that the optimally anti-CRP-immobilized Au nanoplate was able to detect CRP with perfect specificity and attomolar sensitivity. Based on these results, we anticipate that the realization of high-performance biosensors is feasible by optimally immobilizing several bioreceptors on Au nanoplates.

DOI: 10.1021/acsami.9b04363
ACS Appl. Mater. Interfaces 2019, 11, 18960−18967

2. RESULTS AND DISCUSSION

Figure 1a shows a schematic illustration of anti-CRP immobilization onto the Au nanoplate. The ultraflat, ultraclean, and single-crystalline Au nanoplates were synthesized on a sapphire substrate by a simple vapor transport method, as reported previously. The single-crystalline Au nanoplates are triangularly shaped and have 20−30 μm of edge length and 100−200 nm of thickness. The surface of the Au nanoplate was first modified with Cys3-protein G after 12 h of incubation and washing. Three cysteine residues of Cys3-protein G were efficiently bound to the Au surface by Au−S bonding. Next, the anti-CRP was immobilized on the Cys3-protein G-modified Au nanoplate after 12 h of incubation and washing. Because protein G binds specifically to the Fc region of the human IgG antibody, the anti-CRP can be immobilized on the Au nanoplate in the proper orientation for CRP binding. Notably, a previous report suggested that compared with tag-free protein G, Cys3-protein G could improve the antibody binding affinity and antigen detection sensitivity by 4 times and 10 times, respectively. Figure 1b is the AFM topographic image of an Au nanoplate. The surface-height variation in the Au nanoplate is 0.10 nm (R_a) with a 0.13 nm root-mean-square (rms) roughness. Considering that the atomic radius of Au is ~0.14 nm, this value is quite impressive. The AFM results clearly verified that the surface of the Au nanoplate was atomically flat. Figure 1c,d is the AFM images of Cys3-protein G-immobilized and anti-CRP-immobilized Au nanoplates, indicating that Cys3-protein G and anti-CRP are uniformly immobilized onto the atomically flat Au nanoplates.

For the construction of a well-defined anti-CRP-immobilized Au nanoplate, we optimized the Cys3-protein G and antibody immobilization conditions under AFM monitoring. First, the surface of the Au nanoplate was modified with Cys3-protein G over a concentration range from 0.5 to 50 nM (Figures 2a and S1a). When the Au nanoplate was incubated in 0.5 nM of Cys3-protein G solution, the resultant AFM image showed sparsely attached Cys3-protein G residues (bottom panel of Figure 2a). When the Au nanoplate was modified with 5 nM of Cys3-protein G solution, the surface of the Au nanoplate was uniformly and densely coated with Cys3-protein G (middle panel of Figure 2a). From this nanoplate, the height was measured to be 2.09 ± 0.25 nm, and the rms roughness was measured to be 1.34 nm. When the concentration of the Cys3-protein G solution was increased to 50 nM, aggregated proteins were frequently observed on the Au nanoplate, as shown in the top panel of Figure 2a. The height was also increased to 4.28 ± 1.23. Based on the AFM analysis results, we adopted 5 nM of Cys3-protein G solution to optimally modify the surface of the Au nanoplate. Second, anti-CRP was attached on the Cys3-protein G-immobilized Au nanoplate by varying the concentration from 0.3 to 33 nM (Figures 2b and S1b). When the Cys3-protein G-immobilized Au nanoplate was incubated in 0.3 nM of anti-CRP solution, the AFM image shows that the anti-CRP was slightly coated on the Au nanoplate (bottom panel of Figure 2b). When 3 nM of anti-CRP solution was employed, we observed densely and uniformly immobilized anti-CRP on the Au nanoplate (middle panel of Figure 2b). The measured height was 3.28 ± 0.82 nm, and the rms roughness was 1.36 nm. When 33 nM of anti-CRP solution was used, slightly aggregated antibodies were observed. Taken together, we optimally immobilized Cys3-protein G and anti-CRP onto the single-crystalline Au nanoplate through the sequential incubation of Cys3-protein G (5 nM) and anti-CRP (3 nM) solutions.

The optimally anti-CRP-immobilized Au nanoplate may exhibit a highly improved binding ability to CRP. For proof of this ability, we tried to detect CRP by employing the optimally anti-CRP-immobilized Au nanoplate as depicted in Figure 3a.

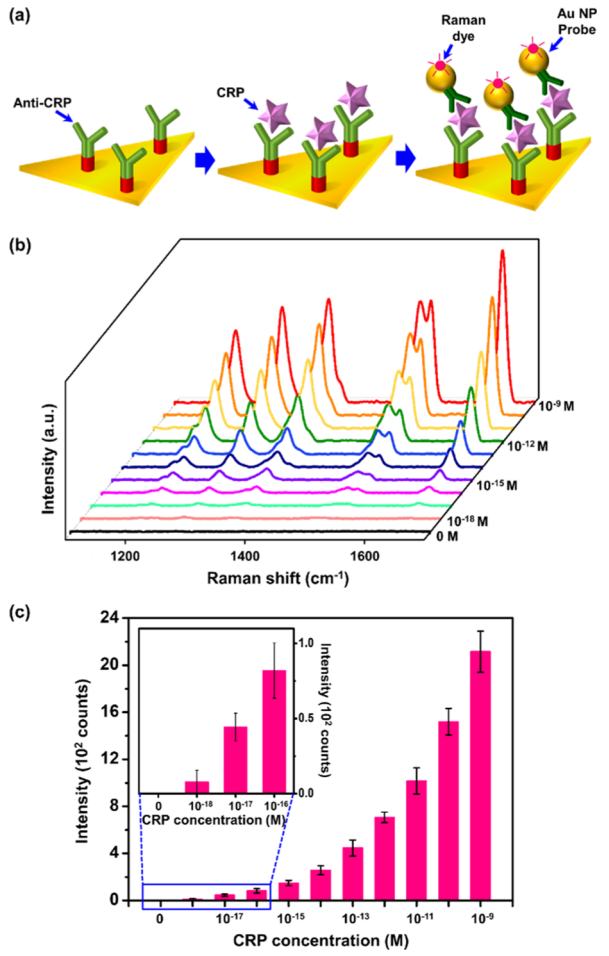

Figure 3. (a) Schematic illustration of CRP detection using an optimally anti-CRP-immobilized Au nanoplate. After preparation of the anti-CRP-immobilized Au nanoplate, the CRP solution was reacted with the nanoplate. Then, anti-CRP-attached Au NP probes were incubated for the construction of the NPs-on-nanoplate architecture. (b) SERS spectra of RBITC obtained from Au NPs-on-nanoplate structures by varying the concentration of CRP from 0 to 10^{-9} M. (c) Plot of the band intensity at 1643 cm^{-1} as a function of the CRP concentration (0−10^{-9} M). The inset is the magnified plot of intensity as a function of CRP concentration (0−10^{-16} M). Data represent the average ± standard deviation from 10 measurements.

After the preparation of the anti-CRP-immobilized Au nanoplates, a variety of concentrated CRP solutions were reacted with the nanoplates and washed thoroughly. Then, Au NP probes were incubated for the construction of NPs-on-nanoplate architectures. Because the Au NPs were also conjugated with anti-CRP, a sandwich immunoreaction can occur between the nanoplate and the Au NP probes in the presence of CRP. In other words, the formation of Au NPs-on-nanoplate structures implies the successful detection of CRP. The Au NPs-on-Au nanoplate structures have been regarded as efficient SERS-active platforms because the SERS signals of molecules can be remarkably enhanced at the nanogaps

DOI: 10.1021/acsami.9b04363
ACS Appl. Mater. Interfaces 2019, 11, 18960−18967

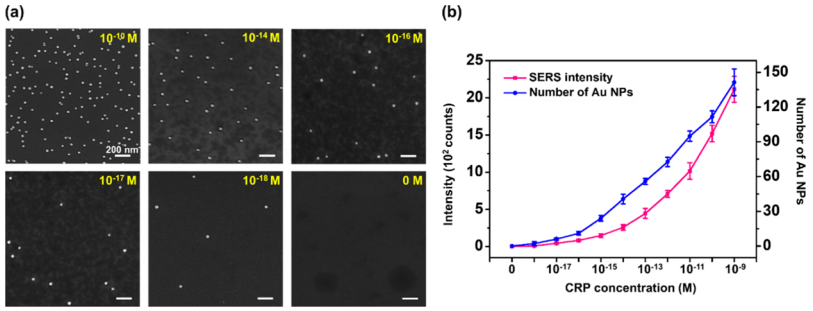

Figure 4. (a) SEM images of Au NPs-on-nanoplate structures at various concentrations of CRP (0, 10^{-18}, 10^{-17}, 10^{-16}, 10^{-14}, and 10^{-10} M). (b) Plot of the band intensity at 1643 cm^{-1} and the number of Au NP probes on nanoplates (1 μm × 1 μm) as a function of the CRP concentration (0–10^{-9} M). Data represent the average ± standard deviation from 10 measurements.

between the two noble metal structures. Hence, we were able to confirm the construction of NPs-on-nanoplate structures, corresponding to the detection of CRP, by measuring the SERS signals. Figure 3b shows the SERS spectra of rhodamine B isothiocyanate (RBITC) obtained from the NPs-on-nanoplate structures by varying the concentration of CRP from 0 to 10^{-9} M. Because the RBITC was attached to the Au NPs only, the strong SERS signals of RBITC clearly proved the formation of NPs-on-nanoplate structures. The peaks are assigned in Table S1. As shown in Figure 3b, the SERS signals gradually increased as the concentration of CRP increased. It is noteworthy that the SERS signals of RBITC were barely detectable when CRP was absent. However, the SERS signals were observable even at an extremely low concentration of 10^{-17} M CRP, corresponding to 5 zmol in a 500 μL sample volume. For quantitative analysis, we plotted the SERS intensity for the 1643 cm^{-1} band as a function of the concentration of CRP (Figure 3c). The raw spectra and fitted line are also shown in Figures S2 and S3. The plot also shows that the SERS intensity gradually increased as the CRP concentration increased from 0 to 10^{-9} M. The inset is the magnified plot of the SERS intensity versus the concentration of CRP from 0 to 10^{-16} M. When the blank samples were tested, no SERS signals of RBTIC were observed. Even though we measured tens of samples, we only obtained noise signals originating from the equipment. This result indicates that the nonspecific adsorption of Au NP probes was significantly suppressed by using the atomically flat Au nanoplates. When the attomolar CRP samples (10^{-18} M) were tested, weak SERS signals of RBITC were observed. Particularly in these samples, we found that the SERS signals blinked according to the measurements. This finding suggests that one or two Au NPs were present in the illuminated area of the Au nanoplate and that, often, no Au NP was in the area of the nanoplate. When the 10^{-17} M CRP samples were employed, we could obtain SERS spectra from all samples without blinking. This result demonstrates that the optimally antibody-immobilized Au nanoplates can detect the antigen at the attomolar level. Considering that the lowest detection limit of CRP was 10^{-16} M,[25] the optimally anti-CRP-immobilized Au nanoplates were able to sensitively detect CRP at an order of magnitude greater than the lowest detection limit.

To further investigate attomolar CRP detection using atomically flat Au nanoplates, we directly observed Au NPs-on-nanoplate structures by SEM. Figures 4a and S4 show the SEM images of Au NPs-on-nanoplates by varying the concentration of CRP. When a CRP sample of 10^{-10} M was used, several well-dispersed Au NP probes were observed on the Au nanoplate. As the concentration of CRP decreased, the number of Au NP probes decreased and finally became zero in the blank sample. This result agrees well with the SERS results for CRP detection, indicating that the Au NPs-on-nanoplate structures can provide enhanced Raman signals of molecules. Figure 4b shows the plots of the SERS intensity for the 1643 cm^{-1} band and the number of Au NP probes versus the concentration of CRP. The number of Au NPs was determined by counting the NPs on the 1 μm^2 nanoplate, corresponding to the laser focused area. From the detection of 10^{-9} M CRP on Au nanoplates, we observed an average of 141.3 Au NP probes. The number of Au NPs decreased as the concentration of CRP decreased, and only 6.0 NPs were found on the Au nanoplate for the detection of 10^{-17} M CRP. Moreover, we found only one or two Au NPs and sometimes zero NPs on the Au nanoplate sensing 10^{-18} M CRP. This observation can explain the blinking SERS signals. After the treatment of blank samples, no Au NP probe was observed on the Au nanoplates. This result suggests that the atomically flat Au nanoplates and optimally immobilized anti-CRP synergistically contributed to the elimination of nonspecific binding of Au NP probes, enabling us to detect CRP at the attomolar level.

The anti-CRP-immobilized Au nanoplates allowed us to detect CRP extremely sensitively by suppressing nonspecific binding. To further explore this specific sensing of CRP, we tried to detect not only CRP but also other proteins, such as bovine serum albumin (BSA), heparin, tumor necrosis factor-α (TNF-α), and Troponin I (cTnI), using optimally anti-CRP-immobilized Au nanoplates. Figure 5a shows SEM images of Au nanoplates after the detection of five kinds of proteins. In the presence of CRP (10^{-9} M), the Au NP probes were well assembled onto the anti-CRP-immobilized Au nanoplate (top panel of Figure 5a), and strong SERS signals of RBITC were obtained (top panel of Figure 5b). In the presence of BSA (8×10^{-9} M), heparin (5×10^{-7} M), TNF-α (10^{-9} M), and cTnI (10^{-9} M), no Au NP probe was found on the nanoplates (middle and bottom panels of Figure 5a), and negligible SERS signals were measured (bottom panel of Figure 5b). This result indicates that the optimally antibody-immobilized Au nanoplates can recognize the target antigen highly specifically and greatly reduce the nonspecific binding of other proteins and even NPs. Because one of the most challenging tasks in immunoassays is to reduce nonspecific binding, the present ultraspecific sensing ability of atomically flat Au nanoplates is quite impressive.

Next, we compared the sensing performances of flat Au nanoplates and rough Au films. Cys3-protein G (5 nM) and anti-CRP (3 nM) were sequentially modified on the Au film

DOI: 10.1021/acsami.9b04363
ACS Appl. Mater. Interfaces 2019, 11, 18960–18967

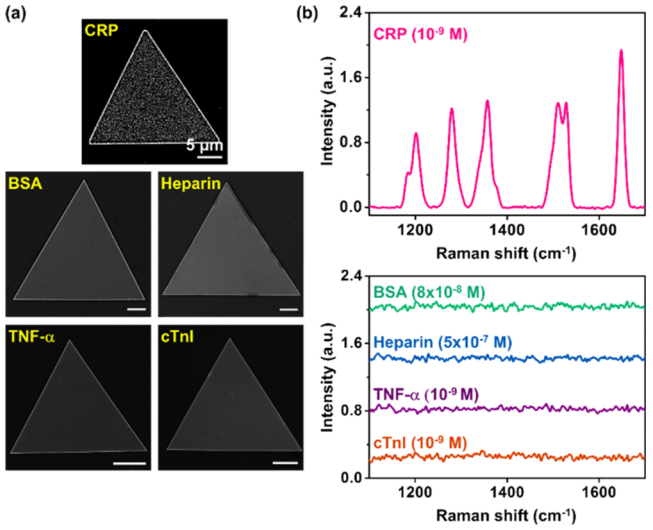

Figure 5. (a) SEM images of Au nanoplates after detection of CRP (10^{-9} M), BSA (8×10^{-9} M), heparin (5×10^{-7} M), TNF-α (10^{-9} M), and cTnI (10^{-9} M). (b) SERS spectra of RBITC obtained from Au nanoplates after detection of CRP (magenta spectrum in the top panel), BSA (green spectrum in the bottom panel), heparin (blue spectrum in the bottom panel), TNF-α (violet spectrum in the bottom panel), and cTnI (orange spectrum in the bottom panel).

through the same procedures as those used for Au nanoplates. Figure S5a is the topological AFM image of the Cys3-protein G-immobilized Au film, showing a height of 5.34 ± 0.98 nm, an R_a value of 1.26 nm, and an rms roughness of 1.60 nm. After the anti-CRP attachment onto the Cys3-protein G-modified Au film, the height, R_a value, and rms roughness increased to 8.24 ± 1.85, 2.70, and 2.08 nm, respectively (Figure S5b). Compared to the AFM images for Au nanoplates, those for the Au film show rougher surfaces. By using anti-CRP-immobilized Au films, we tried to detect CRP. Figures 6a and S6 are the SEM images of Au NPs-on-film structures after the detection of samples with various concentrations of CRP. When the 10^{-9} M CRP sample was detected, several Au NP probes were shown on the Au film. However, the SEM images for the other samples (0–10^{-10} M) showed sparsely distributed Au NPs, making it difficult to quantitatively identify CRP. The plots of the SERS intensity and the number of Au NPs versus the concentration of CRP further showed that the anti-CRP-immobilized Au film could detect CRP at the nanomolar level (Figure 6b). The corresponding full SERS spectra are displayed in Figure S7. Compared to the optimally anti-CRP-immobilized Au nanoplates, the Au films provided a significantly reduced number of Au NP probes and SERS intensities after the detection of CRP. When the 10^{-9} M CRP sample was examined, the average numbers of Au NP probes on the Au nanoplate and the Au film were 141.3 and 59.6, respectively, and the SERS intensities were 2115 and 540, respectively. This difference could be attributed to the fact that more antibodies were immobilized on the flat Au nanoplates than on the rough Au films. Because Cys3-protein G could be assembled uniformly and densely on the atomically flat Au nanoplates, more anti-CRP molecules could be immobilized on the Au nanoplates than on the Au films. Moreover, we found that more nonspecifically attached Au NPs were observed on the Au films than on the Au nanoplates. These nonspecific adsorptions may be caused by van der Waals or electrostatic forces on the partially exposed Au film surfaces. The rough Au films increased the background signals by the nonspecific bindings and decreased the CRP detection signals by sparsely immobilized antibodies, providing a nanomolar sensitivity for CRP. On the other hand, the atomically flat Au nanoplates enabled the attomolar sensing of CRP by the suppression of nonspecific binding and the well-defined immobilization of antibodies.

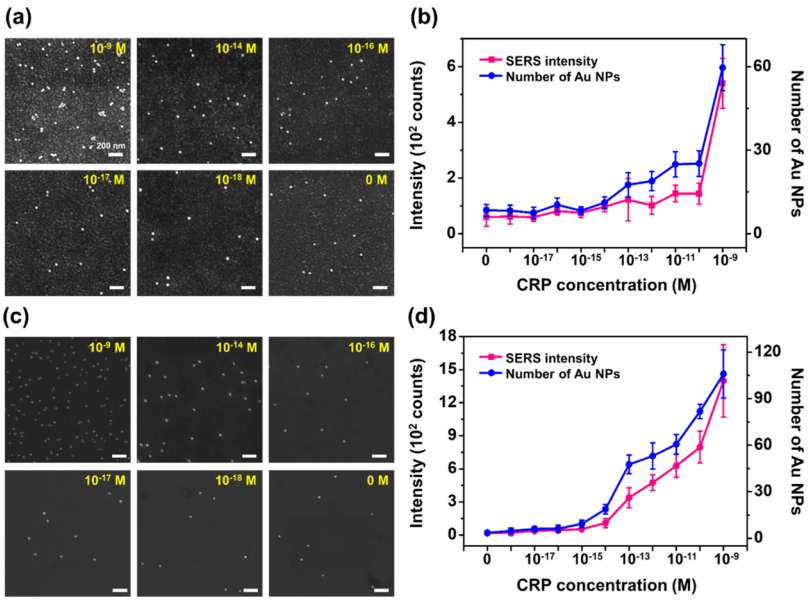

Figure 6. CRP detection results using (a,b) anti-CRP-immobilized rough Au films and (c,d) randomly anti-CRP-immobilized Au nanoplates. (a) SEM images of Au NP-on-film structures at various concentrations of CRP (0, 10^{-18}, 10^{-17}, 10^{-16}, 10^{-14}, and 10^{-10} M). (b) Plot of the band intensity at 1643 cm^{-1} and the number of Au NP probes on films (1 μm × 1 μm) as a function of the CRP concentration (0–10^{-9} M). (c) SEM images of Au NPs-on-nanoplate structures at various concentrations of CRP (0, 10^{-18}, 10^{-17}, 10^{-16}, 10^{-14}, and 10^{-10} M). (d) Plot of the band intensity at 1643 cm^{-1} and the number of Au NP probes on films (1 μm × 1 μm) as a function of CRP concentration (0–10^{-9} M). Data represent the average ± standard deviation from 10 measurements.

DOI: 10.1021/acsami.9b04363
ACS Appl. Mater. Interfaces 2019, 11, 18960–18967

Finally, we tried to detect CRP by employing randomly anti-CRP-immobilized Au nanoplates. For the preparation of anti-CRP with a random orientation, we assembled linker molecules (HS−$(CH_2)_{10}$−NHS) onto the Au nanoplates and then coupled the anti-CRP through the 1-ethyl-3-(3-dimethylaminopropyl) carbodiimide (EDC)/*N*-hydroxysuccinimide (NHS) reaction. The AFM images of the linker molecule-assembled Au nanoplate and the randomly antibody-immobilized Au nanoplate are displayed in Figure S5c,d. After the detection of CRP using randomly antibody-immobilized Au nanoplates, we obtained SEM images of Au NPs-on-nanoplate structures (Figures 6c and S8) and the corresponding SERS spectra (Figure S9). The analyzed plots of the SERS intensity and the number of Au NPs versus the concentration of CRP are also shown in Figure 6d. When the 10^{-9} M CRP sample was detected by using randomly anti-CRP-immobilized Au nanoplates, 105.9 Au NP probes on average were observed. This value is lower than that (141.3) of the optimally anti-CRP-immobilized Au nanoplate but higher than that (59.6) of the rough Au film. As shown in Figure 6d, the number of Au NPs and the SERS intensities decreased as the concentration of CRP decreased from 10^{-9} to 10^{-14} M. Below 10^{-14} M CRP, however, both the SERS signals and the number of Au NPs were undistinguishable. Although the atomically flat Au nanoplates were employed, we might detect CRP at a low concentration of 10^{-14} M with the randomly oriented antibody. Because the well-ordered antibody can improve the antigen binding capacity compared with the random-ordered antibody, this result is reasonable. The comparative experimental results verified that only the optimally anti-CRP-immobilized Au nanoplates make the attomolar detection of CRP feasible. We anticipate that the well-immobilized bioreceptors on the atomically flat Au nanoplates will allow us to realize high-performance biosensors for disease diagnosis and prognosis, environmental monitoring, and food safety.

3. CONCLUSIONS

We report that atomically flat Au nanoplates enable the completely specific and attomolar detection of CRP. Well-defined Au nanoplate-Cys3-protein G-anti-CRP platforms were constructed under AFM monitoring, and then CRP was detected using the platforms. For the confirmation of CRP binding onto the optimally anti-CRP-immobilized Au nanoplates, anti-CRP-attached Au NPs were employed, and SEM and SERS measurements were performed. From the resultant SEM images and SERS spectra, we proved that the atomically flat Au nanoplates remarkably suppressed the nonspecific adsorptions of Au NP probes, allowing us to detect CRP at a low concentration of 10^{-17} M. Moreover, the selectivity test suggested that the optimally antibody-immobilized Au nanoplates could recognize the target antigen accurately. The comparative experiments with anti-CRP-immobilized rough Au films and randomly anti-CRP-attached Au nanoplates further verified that attomolar sensitivity and complete specificity could be synergistically achieved by flat Au nanoplates and the optimal immobilization of the antibody. We expect that atomically flat Au nanoplate platforms can maximize the functionality of biomolecules, thus realizing extremely high-performance biosensors for disease diagnosis and prognosis, environmental monitoring, food safety, and so forth.

4. EXPERIMENTAL SECTION

4.1. Materials. Recombinant human CRP, mouse monoclonal antibody against CRP, sheep polyclonal antibody against CRP, and recombinant human TNF-α were purchased from R&D systems Au slug, Au NPs (20 nm), RBITC, BSA, and heparin sodium salt from porcine intestinal mucosa were purchased from Sigma-Aldrich. Ethanol was purchased from Merck. The phosphate buffered saline (PBS; 10 mM phosphate buffer, pH 7.4, containing 140 mM NaCl) and Tween 20 were purchased from Gibco (Invitrogen). Cys3-protein G was purchased from MiCoBioMed (Korea). The linker molecule (HS−$(CH_2)_{10}$−NHS) was purchased from ProChimia. cTnI and coupling buffer (20 mM Tris-HCl, 300 mM NaCl, 20% (w/v) glycerol, 0.5 mM beta-mercaptoethanol, 0.05% Tween 20, pH 8.0) were kindly provided by POSTECH (Korea).

4.2. Synthesis of Au Nanoplates. The ultraflat, ultraclean, and twin-free single-crystalline Au nanoplates were synthesized in a horizontal hot-wall single-zone furnace system with a 1 in diameter inner quartz tube.[7] The system was equipped with pressure and mass flow controllers. In a quartz tube, an Au slug-containing alumina boat was placed at the center of a heating zone. Before the reaction, the quartz tube was purged with N_2 gas for 30 min to maintain an inert atmosphere, and the pressure was lowered to 5−10 Torr with a gas flow rate of 100 sccm. The Au slug-containing alumina boat was heated to 1100−1170 °C, and the reaction time was 60−90 min. During the reaction, Au vapor was transported by the carrier gas from the high-temperature zone to the low-temperature zone, where sapphire substrates were present. After the reaction, the single-crystalline Au nanoplates could be obtained on the substrates. Au films were prepared by electron beam-assisted deposition of 10 nm Cr followed by 300 nm Au on a Si wafer.

4.3. Immobilization of the Antibody on Au Nanoplates. The single-crystalline Au nanoplates were transferred from the sapphire substrate to a Si wafer by a simple attachment and detachment process with a lubricant of distilled water. The transferred Au nanoplates were incubated in PBS containing 5 nM Cys3-protein G at room temperature for 12 h. After incubation, the Cys3-protein G-modified Au nanoplates were immersed in a 3 nM monoclonal anti-CRP solution for 12 h at room temperature. The resultant anti-CRP-immobilized Au nanoplates were rinsed twice with PBST (10 mM PBS, 0.05% Tween 20, pH 7.4). The same experimental procedure was performed using Au films instead of Au nanoplates for comparison. For the preparation of randomly anti-CRP-immobilized Au nanoplates, the bare nanoplates were incubated in a 1 mM linker molecule-dissolved ethanol solution at room temperature for 12 h. The linker molecule-modified Au nanoplates were immersed in a 3 nM monoclonal anti-CRP solution for 12 h at room temperature and rinsed twice with PBST.

4.4. Detection of CRP Using the Anti-CRP-Immobilized Au Nanoplates. The CRP solution was prepared by dissolving the CRP in a coupling buffer. For the preparation of the Au NP probe solution, an ethanolic solution of RBITC was added to an Au NP solution to a volume of 1 mL with a final RBITC concentration of 1 μM, and this solution was incubated for 1 h at 25 °C. Simultaneously, we prepared a mixture of 10 μL of linker molecule-dissolved ethanol solution (100 μM) and 100 μL of polyclonal anti-CRP solution (1 ng/mL) in an Eppendorf tube for 1 h at 25 °C. Next, 50 μL of the mixture was added to the RBITC-conjugated Au NP probe solution. This solution was incubated for 1 h at room temperature, centrifuged (13 000 rpm) for 15 min, and resuspended in 1 mL of PBST. For the detection of CRP, the prepared CRP solution was added to the anti-CRP-immobilized Au nanoplates or films for 6 h at 25 °C followed by thorough washing with coupling buffer and PBST. Subsequently, the CRP-conjugated Au nanoplates were immersed in an Au NP probe solution at 25 °C for 2 h. The CRP-captured NPs-on-Au nanoplate structures were washed with PBST and distilled water. After drying with N_2 gas, SERS and SEM measurements were performed. The same experimental procedure was performed using BSA, heparin, TNF-α, and cTnI instead of CRP for the selectivity test.

DOI: 10.1021/acsami.9b04363
ACS Appl. Mater. Interfaces 2019, 11, 18960−18967

4.5. Instrumentation. The SEM images were taken on Nova230 (FEI Company). The AFM images were obtained using VEECO and XE-100. The SERS spectra were measured using a high-resolution dispersive Raman microscope (Horiba Jobin Yvon) in which a 633 nm laser with a power of 2 mW was focused on the sample surface with a beam diameter of 1 μm.

■ ASSOCIATED CONTENT

Supporting Information

The Supporting Information is available free of charge on the ACS Publications website at DOI: 10.1021/acsami.9b04363.

SEM images of Au NPs-on-nanoplate structures at various concentrations of CRP (0−10^{-9} M); AFM image of Cys3-protein G-immobilized Au film, anti-CRP-immobilized Au film, linker molecule-immobilized Au nanoplate, and randomly anti-CRP-immobilized Au nanoplate; and CRP detection results by using anti-CRP-immobilized rough Au films and randomly anti-CRP-immobilized Au nanoplates (PDF)

■ AUTHOR INFORMATION

Corresponding Authors

*E-mail: kangtaejoon@kribb.re.kr (T.K).
*E-mail: bongsoo@kaist.ac.kr (B.K.).

ORCID

Jinyoung Jeong: 0000-0003-0381-3958
Eun-Kyung Lim: 0000-0003-2793-3700
Taejoon Kang: 0000-0002-5387-6458
Bongsoo Kim: 0000-0001-5245-4715

Author Contributions

¶A.H. and E.K. contributed equally.

Notes

The authors declare no competing financial interest.

■ ACKNOWLEDGMENTS

This research was supported by the Basic Science Research Program through the National Research Foundation of Korea (NRF) funded by the Ministry of Science and ICT (MSIT) (NRF-2019R1C1C1006867), the Center for BioNano Health-Guard funded by the MSIT of Korea as Global Frontier Project (H-GUARD_2013M3A6B2078950 and H-GUARD_2014M3A6B2060507), the Bio & Medical Technology Development Program of the NRF funded by MSIT of Korea (NRF-2018M3A9E2022821), the First-Mover Program for Accelerating Disruptive Technology Development through the NRF funded by MSIT of Korea (NRF-2018M3C1B9069834) and KRIBB Research initiative Program.

■ REFERENCES

(1) Kang, T.; Yoo, S. M.; Yoon, I.; Lee, S. Y.; Kim, B. Patterned Multiplex Pathogen DNA Detection by Au Particle-On-Wire SERS Sensor. *Nano Lett.* **2010**, *10*, 1189−1193.

(2) Lee, S.; In, J.; Yoo, Y.; Jo, Y.; Park, Y. C.; Kim, H.-j.; Koo, H. C.; Kim, J.; Kim, B.; Wang, K. L. Single Crystalline β-Ag_2Te Nanowire as a New Topological Insulator. *Nano Lett.* **2012**, *12*, 4194−4199.

(3) Huang, J.-S.; Callegari, V.; Geisler, P.; Brüning, C.; Kern, J.; Prangsma, J. C.; Wu, X.; Feichtner, T.; Ziegler, J.; Weinmann, P. Atomically Flat Single-Crystalline Gold Nanostructures for Plasmonic Nanocircuitry. *Nat. Commun.* **2010**, *1*, 150.

(4) Kang, M.; Jung, S.; Zhang, H.; Kang, T.; Kang, H.; Yoo, Y.; Hong, J.-P.; Ahn, J.-P.; Kwak, J.; Jeon, D.; Kotov, N. A.; Kim, B. Subcellular Neural Probes from Single-Crystal Gold Nanowires. *ACS Nano* **2014**, *8*, 8182−8189.

(5) Kang, T.; Choi, W.; Yoon, I.; Lee, H.; Seo, M.-K.; Park, Q.-H.; Kim, B. Rainbow Radiating Single-Crystal Ag Nanowire Nano-antenna. *Nano Lett.* **2012**, *12*, 2331−2336.

(6) Roy, D.; Park, J. W. Spatially Nanoscale-controlled Functional Surfaces toward Efficient Bioactive Platforms. *J. Mater. Chem. B* **2015**, *3*, 5135−5149.

(7) Yoo, Y.; Lee, H.; Lee, H.; Lee, M.; Yang, S.; Hwang, A.; Kim, S.-i.; Park, J. Y.; Choo, J.; Kang, T.; Kim, B. Surfactant-Free Vapor-Phase Synthesis of Single-Crystalline Gold Nanoplates for Optimally Bioactive Surfaces. *Chem. Mater.* **2017**, *29*, 8747−8756.

(8) Lee, M.; Kim, H.; Kim, E.; Yi, S. Y.; Hwang, S. G.; Yang, S.; Lim, E.-K.; Kim, B.; Jung, J.; Kang, T. Multivalent Antibody−Nanoparticle Conjugates To Enhance the Sensitivity of Surface-Enhanced Raman Scattering-Based Immunoassays. *ACS Appl. Mater. Interfaces* **2018**, *10*, 37829−37834.

(9) Vijayendran, R. A.; Leckband, D. E. A Quantitative Assessment of Heterogeneity for Surface-Immobilized Proteins. *Anal. Chem.* **2001**, *73*, 471−480.

(10) Caygill, R. L.; Blair, G. E.; Millner, P. A. A Review on Viral Biosensors to Detect Human Pathogens. *Anal. Chim. Acta* **2010**, *681*, 8−15.

(11) Vo-Dinh, T.; Cullum, B. Biosensors and Biochips: Advances in Biological and Medical Diagnostics. *Fresenius. J. Anal. Chem.* **2000**, *366*, 540−551.

(12) Bae, Y. M.; Oh, B.-K.; Lee, W.; Lee, W. H.; Choi, J.-W. Study on Orientation of Immunoglobulin G on Protein G Layer. *Biosens. Bioelectron.* **2005**, *21*, 103−110.

(13) Neubert, H.; Jacoby, E. S.; Bansal, S. S.; Iles, R. K.; Cowan, D. A.; Kicman, A. T. Enhanced Affinity Capture MALDI-TOF MS: Orientation of an Immunoglobulin G using Recombinant Protein G. *Anal. Chem.* **2002**, *74*, 3677−3683.

(14) Lee, J. M.; Park, H. K.; Jung, Y.; Kim, J. K.; Jung, S. O.; Chung, B. H. Direct Immobilization of Protein G Variants with Various Numbers of Cysteine Residues on a Gold Surface. *Anal. Chem.* **2007**, *79*, 2680−2687.

(15) Jung, Y.; Jeong, J. Y.; Chung, B. H. Recent Advances in Immobilization Methods of Antibodies on Solid Supports. *Analyst* **2008**, *133*, 697−701.

(16) Lee, W.; Oh, B.-K.; Min Bae, Y.; Paek, S.-H.; Hong Lee, W.; Choi, J.-W. Fabrication of Self-Assembled Protein A Monolayer and Its Application as an Immunosensor. *Biosens. Bioelectron.* **2003**, *19*, 185−192.

(17) Akerström, B.; Björck, L. Protein L: An Immunoglobulin Light Chain-Binding Bacterial Protein. Characterization of Binding and Physicochemical Properties. *J. Biol. Chem.* **1989**, *264*, 19740−19746.

(18) Celli, B. R.; Locantore, N.; Yates, J.; Tal-Singer, R.; Miller, B. E.; Bakke, P.; Calverley, P.; Coxson, H.; Crim, C.; Edwards, L. D.; Lomas, D. A.; Duvoix, A.; MacNee, W.; Rennard, S.; Silverman, E.; Vestbo, J.; Wouters, E.; Agustí, A. Inflammatory Biomarkers Improve Clinical Prediction of Mortality in Chronic Obstructive Pulmonary Disease. *Am. J. Respir. Crit. Care Med.* **2012**, *185*, 1065−1072.

(19) Loria, V.; Dato, I.; Graziani, F.; Biasucci, L. M., Myeloperoxidase: A New Biomarker of Inflammation in Ischemic Heart Disease and Acute Coronary Syndromes. *Mediators Inflammation* **2008**, *2008*135625.

(20) Esser, N.; Legrand-Poels, S.; Piette, J.; Scheen, A. J.; Paquot, N. Inflammation as A Link Between Obesity, Metabolic Syndrome and Type 2 Diabetes. *Diabetes Res. Clin. Pract.* **2014**, *105*, 141−150.

(21) Sattar, N.; Scherbakova, O.; Ford, I.; O'Reilly, D. S. J.; Stanley, A.; Forrest, E.; MacFarlane, P. W.; Packard, C. J.; Cobbe, S. M.; Shepherd, J. Elevated Alanine Aminotransferase Predicts New-Onset Type 2 Diabetes Independently of Classical Risk Factors, Metabolic Syndrome, and C-reactive Protein in the West of Scotland Coronary Prevention Study. *Diabetes* **2004**, *53*, 2855−2860.

(22) Ridker, P. M. High-Sensitivity C-reactive Protein and Cardiovascular Risk: Rationale for Screening and Primary Prevention. *Am. J. Cardiol.* **2003**, *92*, 17−22.

DOI: 10.1021/acsami.9b04363
ACS Appl. Mater. Interfaces 2019, 11, 18960−18967

(23) van Wissen, S.; Trip, M. D.; Smilde, T. J.; de Graaf, J.; Stalenhoef, A. F. H.; Kastelein, J. J. P. Differential Hs-CRP Reduction in Patients with Familial Hypercholesterolemia Treated with Aggressive or Conventional Statin Therapy. *Atherosclerosis* **2002**, *165*, 361−366.
(24) Kang, T.; Yoon, I.; Kim, J.; Ihee, H.; Kim, B. Au Nanowire−Au Nanoparticles Conjugated System which Provides Micrometer Size Molecular Sensors. *Chem. Eur J.* **2010**, *16*, 1351−1355.
(25) Wang, S.; Luo, J.; He, Y.; Chai, Y.; Yuan, R.; Yang, X. Combining Porous Magnetic Ni@C Nanospheres and $CaCO_3$ Microcapsule as Surface-Enhanced Raman Spectroscopy Sensing Platform for Hypersensitive C-Reactive Protein Detection. *ACS Appl. Mater. Interfaces* **2018**, *10*, 33707−33712.

DOI: 10.1021/acsami.9b04363
ACS Appl. Mater. Interfaces 2019, 11, 18960−18967